JGR Atmospheres

RESEARCH ARTICLE
10.1029/2023JD040188

Mean Summer Land Temperatures in the Southern California Coastal Zone: Connections With Ocean Processes

M. L. Hale[1], M. A. Merrifield[1], R. E. S. Clemesha[1], A. Gershunov[1], K. Guirguis[1], T. Benmarhnia[1], C. Dorman[1], and S. F. Iacobellis[1]

[1]Scripps Institution of Oceanography, University of California San Diego, La Jolla, CA, USA

Key Points:

- Summer-averaged daily maximum land temperatures exhibit coherent spatial variations across the Southern California coastal plain
- Coastal land temperatures covary with regional ocean temperatures at a similar amplitude, as well as with surface winds and cloud cover
- The number of extreme temperature days in the coastal zone varies with ocean conditions, notably during recent marine heat waves

Supporting Information:

Supporting Information may be found in the online version of this article.

Correspondence to:

M. L. Hale,
m1hale@ucsd.edu

Citation:

Hale, M. L., Merrifield, M. A., Clemesha, R. E. S., Gershunov, A., Guirguis, K., Benmarhnia, T., et al. (2024). Mean summer land temperatures in the Southern California coastal zone: Connections with ocean processes. *Journal of Geophysical Research: Atmospheres*, *129*, e2023JD040188. https://doi.org/10.1029/2023JD040188

Received 11 OCT 2023
Accepted 10 JUL 2024

Author Contributions:

Conceptualization: M. L. Hale, M. A. Merrifield
Data curation: M. L. Hale, M. A. Merrifield, R. E. S. Clemesha
Formal analysis: M. L. Hale, M. A. Merrifield, R. E. S. Clemesha, A. Gershunov, K. Guirguis
Funding acquisition: M. A. Merrifield
Project administration: M. L. Hale, M. A. Merrifield
Visualization: M. L. Hale, M. A. Merrifield

Abstract The cooling effect of the ocean on the Southern California coastal zone is investigated using a high-resolution (4-km) gridded surface meteorological data set (gridMET) of daily maximum temperature (Tmax), with focus on summer mean conditions, taken as the July–August–September (JAS) average. An empirical orthogonal function analysis reveals a coastal mode of JAS temperature covariability, distinct from a more energetic inland mode, that captures Tmax averaged across the Southern California coastal plain. The coastal mode temperature correlates significantly with, and has similar amplitude to, regional sea surface temperature (SST). High (low) summer land and sea surface temperatures, as well as inversion layer temperature differences, are associated with decreases (increases) of northerly coastal wind speeds and coastal cloudiness. The number of extreme heat days on land increases as regional SST increases (4.3 days $°C^{-1}$), with heat wave days 10 times more likely during peak warm versus cool coastal mode years. The coastal zone was notably warmer and heat wave days peaked during the well documented marine heat wave events of 2014/15 and 2018 off Southern California. The marine variability associated with the coastal mode also has strong expression off the Baja California peninsula, presumably due to strong covarying winds in that area. As in previous studies, higher ocean temperatures are attributed to weaker summer winds, with associated reductions in ocean surface heat loss, coastal upwelling, and cloudiness.

Plain Language Summary Summer land temperatures across the Southern California coastal plain are moderated by proximity to the ocean, yet connections between year-to-year changes in summer land and ocean temperatures have not been fully quantified. Averages of July–September temperatures across the coastal plain are well described by a single mode of variability, which contributes to the number of extreme heat days in a given summer. Anomalously warm coastal land conditions are associated with reduced wind speeds and cloud/fog coverage and, most notably, warmer sea surface temperatures over the Southern California Bight and extending southward along the Baja California peninsula. Weak summer winds bring a reduction in ocean surface heat loss, coastal upwelling, and cloudiness, which contribute to higher sea surface temperatures. Strong winds lead to the opposite effect. This study highlights the multiple connections between marine and land heat waves in the SoCal region.

1. Introduction

The cooling effect of the ocean is an important and well-established aspect of Southern California (SoCal) coastal weather and climate (Clemesha et al., 2016; Edinger, 1963; Lebassi-Habtezion et al., 2011). Moderate coastal zone temperatures result from proximity to cool, moist ocean air, marine fog, and coastal clouds. However, the extent to which coastal land and ocean temperatures covary, as well as the co-occurrence of marine heat waves (MHW) and terrestrial heat waves, has not been fully elucidated.

Understanding the drivers of summer temperatures is important for the narrow, densely populated SoCal coastal region, where most SoCal residents live and work (Archer et al., 2018—see their Figure 11), and where extreme heat impacts are substantial (Guirguis et al., 2014, 2018). In addition, Pierce et al. (2018) project ~2.5°C of warming by the middle of the century at the SoCal coast under a high-emissions scenario (RCP 8.5), and ~3.5°C by the end of the century. Coastal heat waves are expected to superpose and intensify on this background warming (Gershunov & Guirguis, 2012), with measured increases in their frequency, intensity, and duration already apparent (Gershunov & Guirguis, 2012; Gershunov et al., 2009, 2021; Kalansky et al., 2018; Messner et al., 2011). A better understanding of the causes of peak temperature variability therefore is a critical and growing concern for the region.

Writing – original draft: M. L. Hale, M. A. Merrifield
Writing – review & editing: M. L. Hale, M. A. Merrifield, R. E. S. Clemesha, A. Gershunov, K. Guirguis, T. Benmarhnia, C. Dorman, S. F. Iacobellis

The above serves as motivation for this study, which aims to further quantify the relationship between ocean and land temperatures in the SoCal region. To do so, we focus on maximum daily temperatures (Tmax) during the hot summer season of the year (July, August, and September—JAS). JAS is chosen as the study period because this is the time of year when Tmax is at its peak in the region and because it provides the strongest expression of the coastal/land covariability that is the concern of this study compared to any other 3-month period.

This work extends prior research regarding the influence of the Pacific Ocean on the climate state of the Southern California coastal region. A ∼300 m thick atmospheric marine layer covers coastal SoCal for much of the year, topped by a deep, dry temperature inversion (Dorman & Winant, 2000; Edinger, 1963). The marine layer temperature and humidity are dictated through contact with the ocean, generally providing cool, moist air to the coastal region (Edinger, 1963). Coastal low clouds and fog, which are common in SoCal particularly in late spring and early summer, are a common feature within the marine layer. Low clouds and fog develop when relatively warm air flows over the cool ocean (Lilly, 1968), or when cool moist marine air mixes upward to reach saturation below a low altitude temperature inversion. Sea surface temperature (SST) is a well-established contributing factor to regional cloudiness (e.g., Filonczuk et al., 1995; Schwartz et al., 2014). The marine layer often traps these low clouds and fog, which act to further cool the region during the day (Clemesha et al., 2016; Iacobellis & Cayan, 2013; Koračin & Dorman, 2001; Small, 2006). Iacobellis and Cayan (2013) found that radiative processes associated with marine strata strongly associate with monthly averages of daily maximum temperature during the summer at SoCal coastal sites. This coastal marine layer phenomenon is affected strongly by topography and distance from the ocean, with the inland extent of coastal fog and clouds in Southern California often being limited by the coastal terrain, particularly the Coast Range mountains (Dorman & Koračin, 2008; Filonczuk et al., 1995; Iacobellis & Cayan, 2013; Schwartz et al., 2014; Small, 2006).

Onshore winds during the summer are a source of moist, cool air for the SoCal coastal plain. The diurnal sea breeze (Lebassi-Habtezion et al., 2011; Sequera et al., 2015) peaks during the day when over-land air temperatures are warm, creating a cross-shore circulation cell that weakens or reverses at night when the land cools. Because the sea breeze circulation depends on the ocean-land temperature difference, ocean processes that affect the SST may also influence land temperatures indirectly. Sequera et al. (2015) note that decadal fluctuations in SST may be an important determinant of summer temperatures within the SoCal Bight/South Coast Air Basin.

Given the influence of SST on coastal cloudiness and circulation, processes that impact the ocean mixed layer heat budget and SST may in turn affect temperatures on land. In general, SSTs off the coast of SoCal are quite cool, due in part to the California Current, which carries water equatorward from the North Pacific (Hickey, 1979). In addition, air-sea heat fluxes, wind-driven vertical transport, and horizontal heat advection drive the upper ocean heat budget in the Southern California Bight (e.g., Zaba et al., 2018). The relative importance of each has been considered in recent heat budget studies of two major MHWs that have impacted the SoCal Bight in the last decade. The first occurred alongside the larger MHW known as the "blob" which began in the North Pacific in 2014 and lasted until 2016 (Fewings & Brown, 2019). This extreme MHW likely resulted from a combination of high downward heat flux (with warm SSTs hampering cloud formation) and unusually weak winds, causing weak upwelling and vertical mixing that further warmed SSTs in the region (Fewings & Brown, 2019; Myers et al., 2018; Robinson, 2016; Zaba & Rudnick, 2016; Zaba et al., 2020). The MHW of 2018 was more localized to SoCal and Baja California (Fumo et al., 2020; Rasmussen et al., 2020; Wei et al., 2021). This event also was linked to wind relaxations, with conflicting views on the relative importance of the surface heat flux (Fumo et al., 2020; Wei et al., 2021).

In this study, we examine year-to-year changes in summer-averaged Tmax in the SoCal coastal zone and consider possible regional connections with the ocean. The coastal temperature pattern of interest has been examined in other contexts (e.g., Abatzoglou et al., 2009—see their Figure 8); however, covariability of this coastal pattern with SST and other marine-related variables has not been explored in such depth. Our goal is to better understand the connections between ocean and land temperatures in this region. First, we describe the SoCal setting and the data and methods used (Section 2). An empirical orthogonal function (EOF) analysis of summer (JAS) averaged Tmax is used to define inland (mode 1) and coastal (mode 2) modes (Section 3.1). We uncover a very strong connection between coastal mode land and ocean temperature variability, that motivates investigation of ocean surface winds, and cloud and fog cover (Section 3.2). We also investigate connections between the coastal summer Tmax pattern and extreme heat events on land in the region (Section 3.3). A discussion (Section 4) follows.

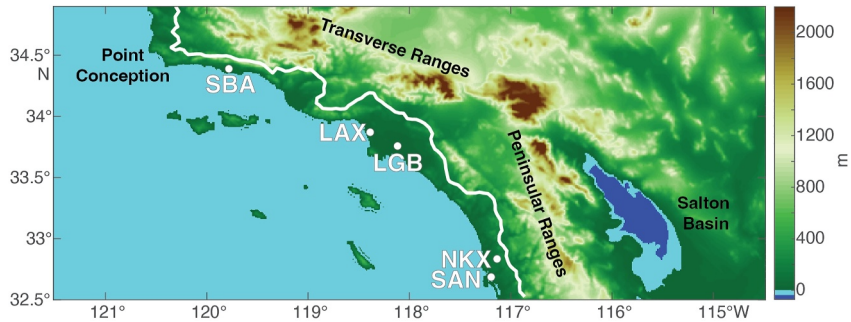

Figure 1. Elevation of the study region with key locations marked. The white contour line indicates the eastern boundary of the "coastal zone" or "mode-2 region" defined in Section 3.1. The mean elevation along this line is 272 m. In situ meteorological time series used in this study are from San Diego International Airport (SAN), Los Angeles International Airport (LAX), Long Beach Airport (LGB), Santa Barbara Municipal Airport (SBA), and Miramar Air Station (NKX).

2. Study Site, Data, and Methods

2.1. Study Site

The Southern California study region (32.48–35°N and 121–115°W, Figure 1) spans, from west to east, the coastal waters of the Southern California Bight, a densely populated coastal plain that stretches 20–30 km inland, the Transverse and the Peninsular Mountain ranges (2,000–3,000 m elevations), and the inland desert region including the low-lying Salton Basin. Seasonal and diurnal variations in temperature are lower at the coast than the mountain and desert regions due to the ocean's moderating influence (McEwen & Brooks, 1923; Planert & Williams, 1995).

2.2. Daily Maximum Temperatures

Daily maximum and minimum temperatures in °C (Tmax and Tmin) from 1979 to 2021 were obtained from gridMET, a 1/24° (~4 km) resolution gridded data set of meteorological variables derived by combining gridded climate data with regional reanalysis (Abatzoglou, 2013). The gridMET database variables have been used in many studies in California, including to assess the compound risk between air pollution and heating days (Masri et al., 2022), to inform water management tools (Melton et al., 2022), to determine how climate and weather factors have contributed to worsening wildfire conditions (Goss et al., 2020), and much more.

2.3. Sea Surface Temperatures

Monthly optimum interpolation SST (OISST) data on a 1° grid spanning 1982–2021 were obtained from the National Oceanic and Atmospheric Administration (NOAA) Physical Sciences Laboratory (Reynolds et al., 2002). The OISST data set is derived from in situ and satellite SST measurements.

2.4. Airport Observations for Temperature and Wind

Other atmospheric data sets include daily surface wind and temperature time series for several airport stations. Daily station maximum temperature data for San Diego International (SAN), Los Angeles International (LAX), Santa Barbara Municipal (SBA), and Long Beach (LGB) airports are obtained from NOAA's National Climatic Data Center (NCDC) Global Historical Climatology Network (GHCN) (Menne et al., 2012a, 2012b). Hourly station temperature, wind speed, and wind direction from the California Automated Surface Observing Systems (ASOS) network for San Diego International (SAN) (as well as for Los Angeles International (LAX), and Santa Barbara Municipal (SBA) airports, and Miramar Air Station (NKX)—all in Supplemental Materials only), are obtained from Iowa Environmental Mesonet (ASOS User's Guide, 1998). The airport time series span 1979–2021. We use the daily station temperature time series to complement and check the gridMET data set, which we find is well suited for investigating year-to-year variability.

2.5. Coastal Low Clouds and Fog and ERA5 Reanalysis Data

Monthly 4-km resolution low-level cloud/fog coverage spanning May–September of 1996–2020 for the region 25–50°N, 130–113°W were retrieved from NASA/NOAA Geostationary Operational Environmental Satellite (GOES) (Clemesha et al., 2016). These data measure the percent time of day and night that low clouds/fog are present. Monthly averaged 10 m winds on a 0.25° resolution grid spanning 1979–2021 were obtained from the ECMWF Reanalysis v5 (ERA5) database through the Copernicus Climate Data Store (Hersbach et al., 2020).

2.6. Climate Indices

Monthly Pacific climate indices used in this study include the Oceanic Niño Index (ONI) (1979–2021), the Niño 3 SST Index (1979–2021), the Pacific Decadal Oscillation (PDO) index (1979–2021), and the North Pacific Gyre Oscillation (NPGO) index (1979–2018). The ONI, obtained from the NOAA Climate Prediction Center, is based on Niño 3.4 region 3-month running-mean SST anomalies from a historical reconstructed SST analysis (Extended Reconstructed SST—ERSST.v5) (Huang et al., 2017). The Niño 3 SST Index was obtained from NOAA Physical Sciences Laboratory Global Climate Observing System (GCOS) Working Group on Surface Pressure (WG-SP) and is calculated using the HadISST1 data set (Rayner et al., 2003). The PDO index, obtained from the NOAA National Centers for Environmental Information (NCEI), combines the Mantua PDO index (Mantua et al., 1997) with ERSST.v5 (Huang et al., 2017). The NPGO index, obtained from Emanuele Di Lorenzo's NPGO webpage (Di Lorenzo et al., 2008), is derived from Northeast Pacific (25–62°N, 180–110°W) sea surface height variability.

2.7. Inversion ΔT

Temperature inversion time series from Miramar Air Station (NKX) were obtained from the NOAA Earth System Research Laboratories Radiosonde Database (Schwartz & Govett, 1992). The inversion ΔT, or inversion strength, measurement is defined as the difference in temperature (°C) from between the top and bottom of the inversion layer, as in Clemesha et al. (2018) and Iacobellis et al. (2010).

2.8. Heat Wave Days

In this study, we defined "heat wave days" as days when daily Tmax exceeds a 95th percentile threshold computed following the methodology of Hulley et al. (2020), which is based on Perkins et al. (2012). Hulley et al. (2020) use the WMO 1961–1990 baseline to determine percentiles, whereas we use the full Tmax time series (1979–2021). Ninety-fifth percentile thresholds for each day of the JAS season are specified for Tmax (named Tmax95), defined based on the temperatures of that individual day and the 7 days before and after. This rolling threshold definition is implemented to account for the seasonally changing climatology within the JAS period. Similar results were obtained using the heating day index defined by Gershunov et al. (2009). The heat wave days analysis (Section 3.3) is applied to daily Tmax from the GHCN temperature time series. Comparing heat wave days obtained from the GHCN stations with the gridMET data at the closest grid point to each GHCN station yielded qualitatively similar results; however, the gridMET data exhibited a small increase in Tmax variance over the section of data that has been updated (after 2011) since the original gridMET data reported in Abatzoglou (2013).

2.9. EOF and the Generalized Extreme Value Distribution

We used EOF analysis applied to gridMET Tmax to identify the coastal and inland zones and to quantify interannual temperature variability. The resulting EOFs provide dominant patterns of Tmax variability. The second mode defines the spatial extent of the coastal zone and its associated temporal behavior. EOFs are computed for JAS-averaged time series after removing the temporal mean and linear trend at each grid point. For each mode j, the temporal ($A_j(t)$) and spatial ($E_j(x)$) components have been normalized so that the corresponding temporal expansions can then be interpreted as the change in average temperature (°C) in the respective zones. Similar results are obtained if the seasonal cycle also is removed prior to forming the JAS-averages, and if the linear trend is included, as Tmax trends generally are weak over the study period. Linear trends are stronger in some of the other variables considered (e.g., SST), and so to focus on year-to-year as opposed to longer-term change, we remove a linear trend from all variables prior to computing correlations and regressions.

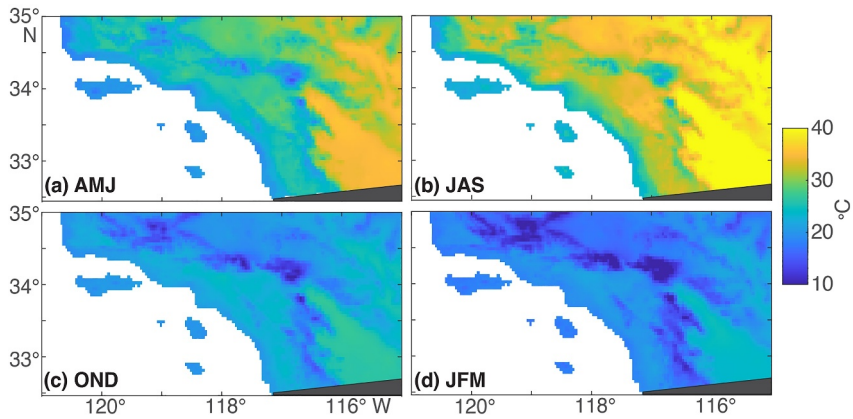

Figure 2. (a) Spring/AMJ, (b) Summer/JAS, (c) Fall/OND, and (d) Winter/JFM mean Tmax (°C) for the study region. Tmax is averaged over the period spanning 1979–2021. A distinctive cool (~20–25°C) coastal strip is present in the summer mean Tmax map. The temperature scale has been set as the range from 10 to 40°C; therefore, maximum and minimum values may exceed the limits shown here.

Daily Tmax data from the GHCN stations were fit to a Generalized Extreme Value (GEV) distribution (Coles, 2001) for each JAS summer period to characterize how extremal Tmax statistics vary with the JAS-averaged Tmax in the coastal zone. For our parameter ranges, the GEV cumulative distribution function is given by $F(x) = e^{-t(x)}$, where $t(x) = [1 + \xi((x - \mu)/\sigma)]^{-1/\xi}$, where here x is the 14 highest Tmax values of a given summer, assuming a spacing of at least 3 days between independent Tmax values. The function gevfit in MATLAB is used to obtain the location (μ), scale (σ), and shape (ξ) parameters. In the application to the SAN station data, 2 summers out of 43 were excluded from the analysis because the maximum likelihood estimation in gevfit did not converge.

3. Results

3.1. Definition of the Southern California Tmax Coastal Mode

Seasonally, the moderating influence of the ocean on SoCal coastal plain temperatures is evident in spring and summer (Figure 2); however, the contrast is strongest during the summer days, when JAS-averaged Tmax levels in a thin strip near the coast are 10–20°C cooler than areas further inland, including some areas west of the mountains (Figure 2b). Relatively cool summer Tmax temperatures also appear at higher mountain elevations separating the coastal zone from the desert region. In contrast, during the winter (January–March, JFM, Figure 2d), average Tmax values in the coastal and inland-coastal areas (west of the mountains) generally are within 10°C of each other, and the coastal strip is not distinct. For the remainder of this study, we will focus on Tmax summer/JAS conditions, when the coastal-inland contrast is at a seasonal high.

To quantify this inland-coastal temperature contrast and to examine how average summer temperatures along the coast vary from year to year, we employ an EOF analysis of JAS-averaged Tmax. The first two modes account for ~75% of the total variance (Figure 3). Mode 1 (51.23% of the total variance) describes coherent variation over the inland mountain and desert zones with weak expression near the coast (Figure 3a), and mode 2 (24.99%) describes a complementary pattern with high amplitudes along the coastal plain and offshore islands and weak amplitudes inland (Figure 3b). These two spatial modes, $E_1(x)$ and $E_2(x)$, are near inverses of one another. A clear inland/coastal separation also appears in r^2 of observed Tmax and mode 2 at each grid point, with mode 2 dominating the variability in the coastal zone (Figure 3d), and mode 1 primarily accounting for inland variability (Figure 3c). EOF analyses of average and minimum daily temperatures produce some similar low mode patterns as Tmax, although the coastal versus inland mode patterns are the most distinct when using Tmax, and the variance explained by mode 2 is reduced in Tmin or Tavg EOFs (for an EOF of Tmin, see Figure S1 in Supporting Information S1). EOFs performed for other seasons generally show a similar but weaker coastal pattern as in summer.

Given the clear distinction between the spatial patterns of the two modes (Figures 3a and 3b) and the variability that they describe (Figures 3c and 3d), we divide the study region into a "coastal zone" and an "inland zone." The

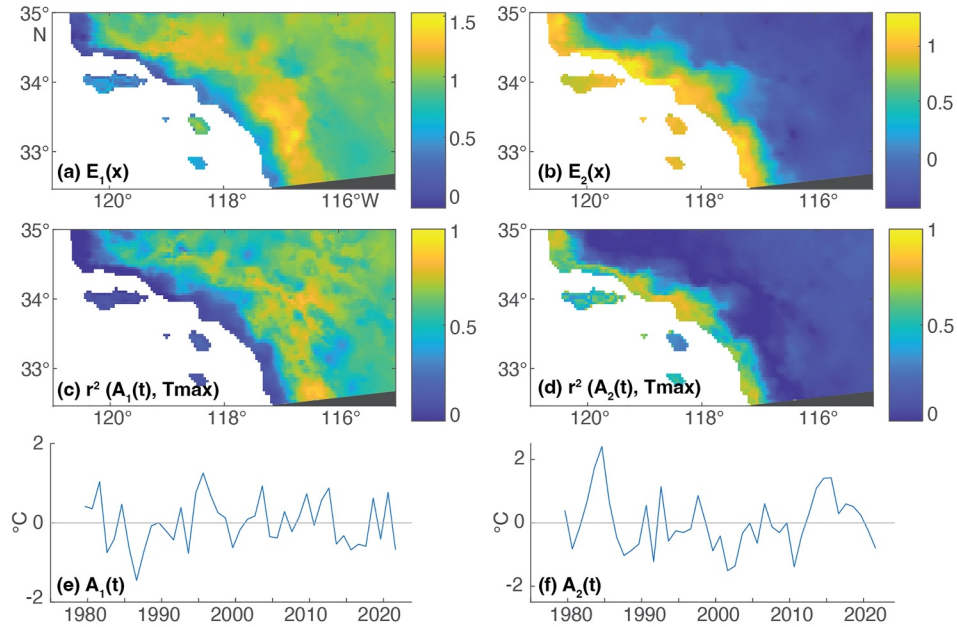

Figure 3. Empirical orthogonal function results of the JAS-averaged Tmax for 1979–2021. Figures on the left correspond to mode 1 (inland mode); figures on the right correspond to mode 2 (coastal mode). From top to bottom: spatial modes showing a distinct (a) inland ($E_1(x)$) versus (b) coastal ($E_2(x)$) pattern, r^2 of observed Tmax with (c) $A_1(t)$ and (d) $A_2(t)$, and temporal expansions (e) $A_1(t)$ and (f) $A_2(t)$. Note that time series points in this figure (and other time series herein) are centered in August, while the *x*-axis ticks indicate the start of each year.

coastal zone is defined as the region where mode 2 amplitudes ($E_2(x)$) exceed 0.8, roughly corresponding to the yellow strip in Figure 3b and depicted in Figure 1. The inland zone is the remaining land area. This cutoff was selected because it encompasses a coastal plain region where the mode-2 amplitudes are spatially homogeneous; further inland of this line the mode-2 amplitudes begin to fall quickly as the terrain moves to higher elevation. We include the inland mode to highlight separation of the two zones; however, the coastal mode is the main interest of our study. Each mode's temporal and spatial components have been normalized so that the spatial average of $E_1(x)$ across the inland zone equals to one, and the same for $E_2(x)$ averaged in the coastal zone. The temporal expansions $A_1(t)$ and $A_2(t)$ (Figures 3e and 3f) can then be interpreted as the change in average temperature (°C) in the respective zones. For example, the spatial average of JAS Tmax in the coastal zone was >2°C warmer in 1984 (Figure 3f). The coastal mode temporal amplitude ranges from year to year from −1.5°C to +2.4°C.

Because the coastal mode explains such a high fraction of variability in the coastal zone (Figure 3b) and given the normalization imposed, it follows that $A_2(t)$ correlates with summer Tmax spatially averaged in the coastal zone ($r = 0.91$). Thus $A_2(t)$ can be treated as of the mean summer Tmax in the coastal zone, with $E_2(x)$ capturing spatial variations of that mean signal. For example, the range of $E_2(x)$ amplitudes (0.8–1.2 within the coastal zone) indicates that the coastal mode signal varies spatially by approximately ±20%. We use the JAS mode 2 temporal expansion ($A_2(t)$, Figure 3f) as our indicator of year-to-year changes in mean daily maximum temperatures in the Southern California coastal zone during the hottest time of the year. Of interest are the oceanic and atmospheric variables that covary with the coastal Tmax variability captured by mode 2.

Having defined coastal and inland zones, we compare seasonal climatologies of Tmax averaged within these zones (Figure 4). The three hottest months for monthly mean Tmax occur in July, August, and September (JAS) in the coastal zone, compared to June, July, and August (JJA) in the inland zone. The delayed summer peak in the coastal zone relative to the inland zone also was noted by Gershunov and Guirguis (2012). The seasonal climatology of SST, computed here from the OISST gridded product, peaks in August, September, and October, suggesting that the delay of the coastal zone seasonal temperature relative to inland could be connected to the ocean. In addition to the timing of the peak, the flattened shape of the Tmax coastal curve more closely resembles the shape of the SST curve than the shape of the inland Tmax curve, which has a much larger range.

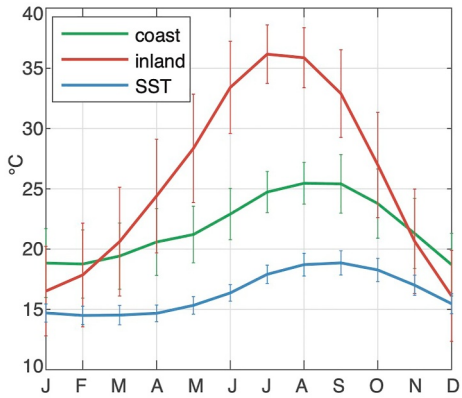

Figure 4. Mean monthly Tmax for coastal (green line) and inland (red line) zones, and sea surface temperature (SST) (blue line), 1979–2021. Coastal and inland zones were defined based on Figure 3b. Mean monthly SST is calculated from an average of 8 total SST grid cells in the SoCal Bight: [32.5°N, 120.5°W], [32.5°N, 119.5°W], [32.5°N, 118.5°W], [32.5°N, 117.5°W], [33.5°N, 120.5°W], [33.5°N, 119.5°W], [33.5°N, 118.5°W], [34.5°N, 120.5°W]. Error bars represent ±one standard deviation.

3.2. Covariations With the Tmax Coastal Mode

To investigate what factors determine the time dependence of the coastal mode, we explore correlations with potential climate drivers and regional variables. The coastal mode pattern does not strongly correlate with the Pacific climate indices PDO, ONI, Niño 3, and NPGO. The only statistically significant correlation ($p < 0.05$) is between A_2(t) and JAS averages of the PDO, though the correlation is weak ($r = 0.38$). The correlations between A_2(t) and JAS ONI ($r = 0.22$), A_2(t) and JAS Niño 3 ($r = 0.30$), and A_2(t) and JAS NPGO ($r = -0.28$) are even weaker. A low correlation between the coastal mode and the PDO index occurs for different lead times of the PDO relative to the coastal mode. Alfaro et al. (2006) similarly found low correspondence between the PDO and early summer (JJA) Tmax over the western United States using a canonical correlation analysis, although stronger connections were noted between Tmin and the PDO.

High correlations are found, however, between the coastal mode and regional ocean-related variables. Gridded spatial correlation maps between A_2(t) and SST, cloud/fog cover, and wind speed over the ocean depict an area of high correlation in the waters offshore from the Baja California peninsula (Figure 5). The correlation with SST (Figure 5a) is highest in the waters off this peninsula, as well as extending north into the waters off Southern California. North of the SoCal Bight, the correlation weakens slightly before completely tapering off around 39°N (not shown). A similar SST pattern from Point Conception to Baja California was identified by Alfaro et al. (2006) and related to SoCal summer land temperatures (JJA). Correlation coefficients also are high in the negative direction between A_2(t) and percent cloud/fog cover in the SoCal Bight and off the coast of the northern half of the Baja California peninsula (Figure 5b), and these high correlation coefficients also extend south, though they seem to taper off somewhat around 26°N (the gridded low cloud/fog data are not available south of 25°N). The low cloud/fog correlation does not continue north of Point Conception. The wind spatial correlations with A_2(t) (also negative) (Figure 5c) peak in strength off the coast of the Baja California peninsula and weaken within the SoCal Bight region.

We note that the coastal mode and SST fluctuations are not only strongly correlated, but they have very similar amplitudes (Figure 6a), highlighting the strong linkage between local SST and land temperature changes at the SoCal coast. A_2(t) therefore not only represents year-to-year fluctuations of the mean JAS Tmax across the land coastal zone, but of the mean coastal ocean surface temperatures as well. A strong anti-correlation is also found between A_2(t) and the inversion ΔT measured at NKX (Figure 6b), reflecting that this temperature difference is dominated by changes in the surface temperature, represented by coastal mode variability. Additionally, there is a strong anti-correlation between A_2(t) and percent cloud/fog cover (Figure 6c), suggesting the modulating influence of clouds/fog, as expected. The high correlations with inversion ΔT and clouds/fog make sense given the

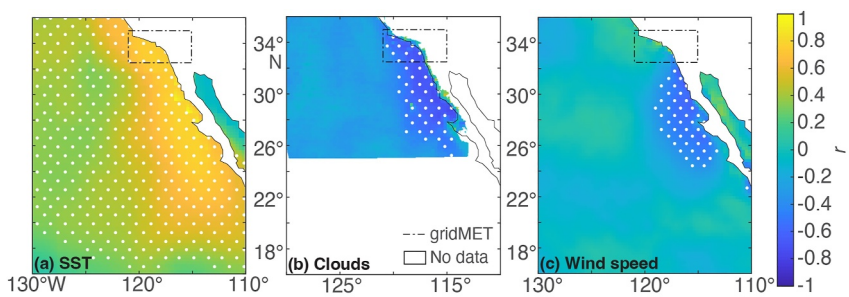

Figure 5. Gridded spatial correlation maps between A_2(t) and (a) sea surface temperature (SST), (b) coastal low clouds and fog, and (c) wind speed. The dashed black box indicates the gridMET study region (as in Figures 2 and 3). In general, correlations are significant at the 95% significance level when $|r| > 0.32$ (SST), 0.40 (clouds/fog), 0.31 (wind). White stippling represents areas of statistical significance. For stippling, we utilized the MATLAB stipple function available on MathWorks File Exchange (Greene, 2024).

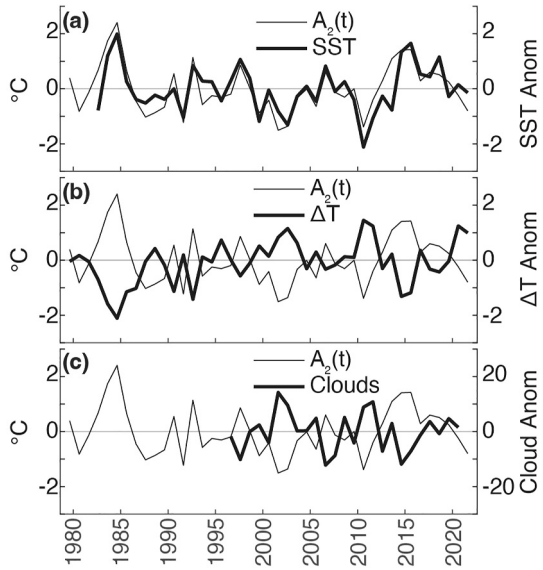

Figure 6. Time series of $A_2(t)$ compared with JAS-averaged (a) sea surface temperature (average of four grid cells at coordinates [32.5°N, 118.5°W], [32.5°N, 117.5°W], [33.5°N, 119.5°W], and [33.5°N, 118.5°W]; $r = 0.79$), (b): inversion ΔT (32.9°N, 117.1°W; $r = -0.80$), and (c): percent low cloud/fog cover (32.97°N, 117.5°W; $r = -0.70$).

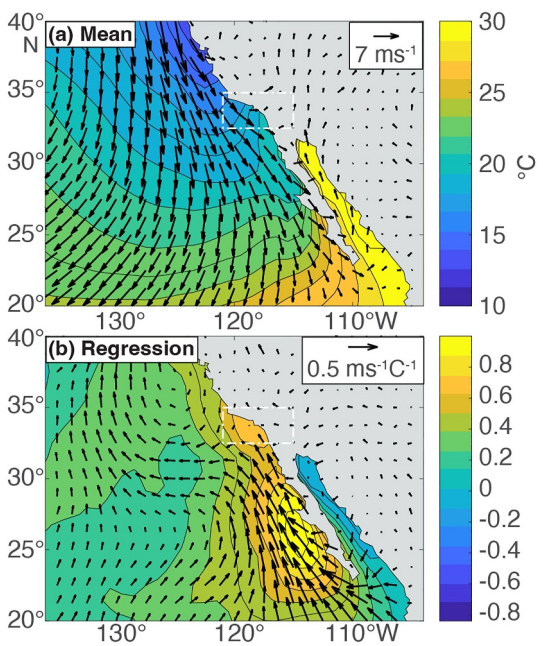

Figure 7. (a) JAS-averaged surface wind vectors overlaid on sea surface temperature (SST). (b) Regression map of JAS-averaged surface winds and SST regressed on $A_2(t)$. The dashed white box indicates the gridMET study region (as in Figures 2 and 3). Due to the density of ERA5 wind data, only every fifth wind vector is plotted.

strong correlation between $A_2(t)$ and ocean temperatures, as the inversion layer and clouds are themselves linked to the ocean in this region.

The highest amplitude wind, SST, and cloud/fog cover changes associated with the coastal mode signal occur off Baja California. On average during JAS, winds along the SoCal coast are northwesterly and SSTs exhibit a southward penetration of cool waters from the north associated with the California Current (Figure 7a, also Winant & Dorman, 1997). A nearly 10° meridional difference in SST occurs between the southern tip of the Baja California peninsula and Point Conception. Mean JAS winds in the SoCal Bight generally are weaker than those further offshore, or in the coastal areas north and south of the bight. The coastal mode is associated with a weakening of the northwesterly winds off Baja California (i.e., warmer coastal temperatures are associated with weaker winds), evident in Figure 7b as a southeasterly anomaly when $A_2(t)$ is positive. Below this wind anomaly in Figure 7b is the strongest expression of SST associated with $A_2(t)$, showing a warming of the surface ocean linked to decreased wind speeds. Wind relaxations in this region have been linked to MHWs (Fewings & Brown, 2019; Fumo et al., 2020; Robinson, 2016; Wei et al., 2021; Zaba & Rudnick, 2016; Zaba et al., 2020), and to poleward coastal current anomalies (Durazo, 2015; Melton et al., 2009; Oey, 1999; Vazquez & Gomez-Valdes, 2018).

Because of the connection between SST and winds, we next investigate whether years of high/low coastal mode amplitude (i.e., warm/cold coastal summer temperatures) correspond to a weakening/strengthening of the summer SoCal ocean-land marine air exchange, either on average or through changes in the diurnal sea breeze. Given the important role of sea breeze in the climate of the SoCal coastal region, including findings that the strength of onshore winds increases as the land-ocean temperature gradient increases (Lebassi-Habtezion et al., 2011), we hypothesize that the advection of cool, moist marine air onto the SoCal coastal plain via cross-shore circulations at daily or longer time scales accounts for the strong resemblance between SST and land temperatures (Figure 6a). For this analysis, we investigate hourly wind and temperature time series at ASOS airport stations within the coastal zone to attempt to discern changes in mean or diurnal behavior associated with $A_2(t)$ years. Figure 8a depicts the daily summer sea breeze at SAN (using the oceanographic convention with positive u directed onshore), which peaks in the afternoon and weakens during the evening. Figure 8b depicts daily temperatures measured at the same station. Both plots depict JAS averages for each hour of the day composited by years with positive/warm (1982, 1983, 1984, 1985, 1992, 1997, 2006, 2013, 2014, 2015, 2017) and negative/cool (1980, 1987, 1988, 1989, 1991, 1993, 1999, 2001, 2002, 2005, 2010, 2021) $A_2(t)$ amplitude. We find that the onshore wind speeds at each station are similar between warm and cool coastal mode summers (Figure 8a), hence we discount that the coastal mode variations reflect a strengthening or weakening of the sea breeze, or the mean onshore circulation during summer. In terms of temperature (Figure 8b), we observe that warm/positive $A_2(t)$ years correspond to warmer temperatures throughout the day compared to cold/negative years. Our study has focused on the peak daily temperature (Tmax), but Figure 8b indicates that the summer warming and cooling affects all hours of the day, not only during the midday hours of maximum temperatures. Based on Figure 8, we conclude that changes in $A_2(t)$ do not simply lead to changes in the strength of either the summer mean or diurnally varying winds, that is, warmer land temperatures don't necessarily drive a stronger onshore circulation. Because changes in $A_2(t)$ correspond to changes in air temperatures nearly uniformly throughout the day (Figure 8b), it is unlikely that diurnal

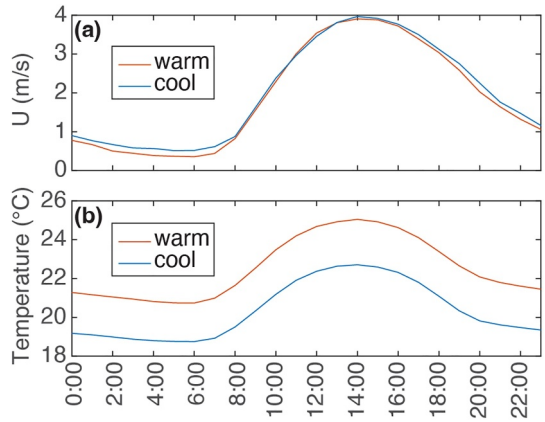

Figure 8. (a) East-west winds (U) measured at SAN averaged over years of positive/warm (1982, 1983, 1984, 1985, 1992, 1997, 2006, 2013, 2014, 2015, 2017) and negative/cool (1980, 1987, 1988, 1989, 1991, 1993, 1999, 2001, 2002, 2005, 2010, 2021) A_2(t) amplitude, for each hour of the day (Pacific standard time). At SAN, U winds are in the cross-shore direction. (b) Temperature measured at the same station and years.

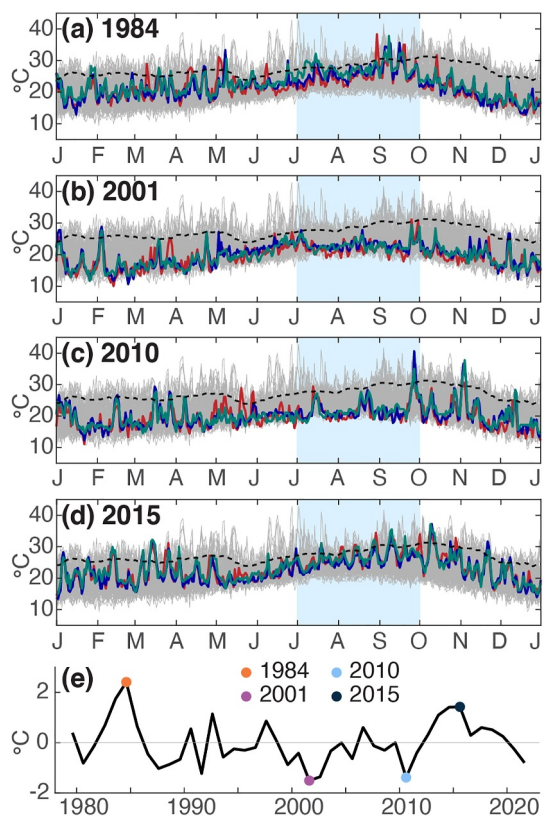

Figure 9. Tmax in the coastal zone for all years (gray) and specific extrema years (colored lines of a–d). Green indicates SAN, blue indicates LAX, and red indicates SBA. The JAS season is highlighted in pale blue. Colored circles on the A_2(t) time series (e) denote the chosen example years. The dashed line on all subplots indicates Tmax95, or the daily 95th percentile threshold for Tmax.

changes in the surface radiation budget (e.g., changes in cloud/fog cover over land during the morning hours) could account for coastal zone temperature variability. Although our focus has been on Tmax based on the availability of the gridMET data set, the marine influence on coastal land temperatures occurs throughout the day and night. Similar results are found for LAX (Figure S2 in Supporting Information S1), NKX (Figure S3 in Supporting Information S1), and SBA (Figure S4 in Supporting Information S1).

3.3. The Tmax Coastal Mode, Variability, and Summer Heat Waves

Our findings indicate connections between ocean variables and coastal zone temperatures averaged over the summer, but does this variability also impact extreme heat events on land? Illustrative daily Tmax time series for coastal mode extrema years, using GHCN airport station data, show that the coastal mode primarily captures changes in the baseline summer Tmax, superposed on which are ∼week-long warm events, sometimes reaching heat wave intensities (Figure 9). JAS temperatures for 1984 (a coastal mode maximum year) are average to warmer than average for the observation period (1979–2021) and reach record highs in late August and September (Figure 9a). A downward shift in baseline Tmax occurs during JAS 2001 (a coastal mode minimum year), with temperatures at the stations reading below average (Figure 9b). Another minimum coastal mode year (2010, Figure 9c) also illustrates a very low baseline Tmax, with daily JAS temperatures near the lowest on record, though punctuated by a handful of warm events including a record heat wave in late September. 2015 (Figure 9d) is another maximum coastal mode year, and, like 1984, has a warmer-than-average baseline Tmax. Note that these results reflect mean values, and not necessarily individual heating events. For example, the highest Tmax value recorded over the observation period occurred in September 2010, an otherwise very cool coastal mode year. The in-situ airport data and gridded products yield similar versions of Figure 9.

In addition to describing the mean coastal zone temperature, there is a relationship between the coastal mode and the number of heat wave days that occur within the coastal zone each summer. To illustrate this connection, we determine the number of heat wave days at four GHCN stations located within the coastal zone (SAN, LAX, SBA, LGB) using the Tmax95 heat wave threshold definition described in Section 2 (as applied to each of the stations individually) and summing the number of days that exceed the Tmax95 threshold (computed over JAS for all years). The values are then averaged across all four stations. The number of heat wave days (Figure 10b) correlates significantly with A_2(t) (Figure 10a) ($r = 0.73$, $p < 0.05$), with large peaks in the early–mid 1980s and mid–late 2010s, and distinct troughs in the late 1980s, early 2000s, and, to a lesser extent, early 2010s.

One reason for the connection between mean and extreme temperatures is that a change in the mean temperature corresponds to a warm-shift of the underlying temperature probability distribution, which we see in daily Tmax for the coastal zone for the 4 warmest and coolest A_2(t) years (Figure 11a). To better quantify that relationship, we apply a GEV fit to the SAN daily Tmax record. A GEV distribution is fit to the 14 highest Tmax days during the JAS summer months for each year of the record. We find that A_2(t) correlates significantly ($p < 0.05$) with the shape ($r = -0.41$), scale ($r = 0.40$), and location ($r = 0.75$) parameters of the fitted GEV distributions. The relatively high correlation with the location parameter reinforces the visual impression in Figure 11a that warm A_2(t) years result in a warm shift of the GEV

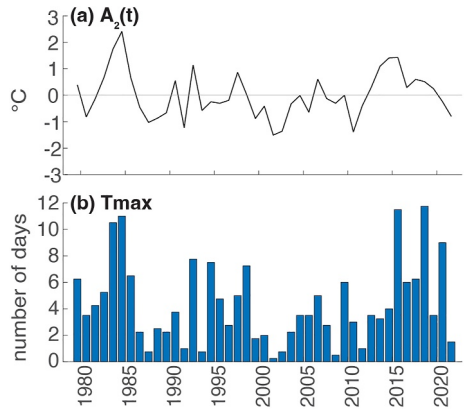

Figure 10. (a) A_2(t) versus (b) Days above the Tmax95 threshold for each JAS season, average of four stations within the coastal zone (SAN, LAX, SBA, LGB). $r = 0.73$.

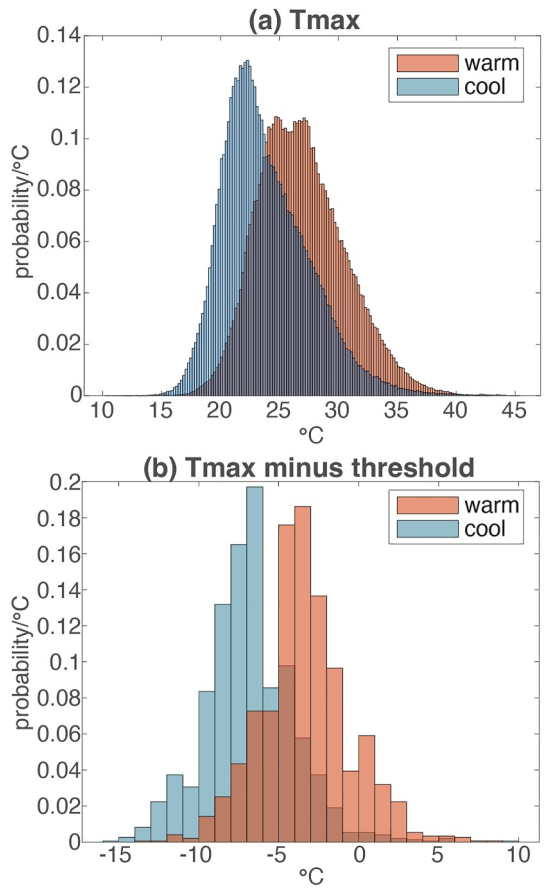

Figure 11. (a) Probability distribution functions of gridMET Tmax in the coastal zone for four positive (warm) A_2(t) years (red bars, 1983, 1984, 2014, 2015) and four negative (cool) A_2(t) years (blue bars, 1991, 2001, 2002, 2010). (b) Tmax95 threshold exceedance for four GHCN airport stations (SAN, LAX, LGB, SBA) for four positive (warm) A_2(t) years (red bars, 1983, 1984, 2014, 2015) and four negative (cool) A_2(t) years (blue bars, 1991, 2001, 2002, 2010).

distribution. At the other GHCN stations, the gevfits result in weak and variable correlations with A_2(t) for shape (0.1 to −0.2) and scale (0.14–0.44), whereas the correlations with the location parameter remain relatively high (0.62–0.70) although weaker than SAN.

How do the number of heat wave days in a given summer vary with the coastal mode? Figure 11b shows the exceedance over the Tmax95 threshold for four specific GHCN stations (SAN, LAX, SBA, LGB) within the gridMET coastal region. A specific Tmax95 threshold was defined for each of these stations and the number of days in which Tmax exceeds this threshold was calculated for each of these stations in the four warmest (1983, 1984, 2014, 2015) and four coolest (1991, 2001, 2002, 2010) A_2(t) years. Anything greater than zero on the *x*-axis of Figure 11b represents a heat wave day. It is apparent from Figure 11b that heat wave days are more common in warm A_2(t) years. In fact, the probability of a heat wave is an order of magnitude greater during the four warmest A_2(t) years (0.10) than during the four coolest A_2(t) years (0.01).

4. Discussion and Conclusions

The coastal mode Tmax pattern represents ocean-influenced coastal zone temperature variability. This pattern is strongly tied to SST in terms of correlation and amplitude. Coastal Tmax also correlates strongly with ocean-related variables including cloud and fog cover and wind anomalies. These phenomena are each interrelated with one another. For example, cooler (warmer) SSTs tend to result in more (fewer) low-level clouds/fog (Schwartz et al., 2014; Wang et al., 2002), and warm SSTs are sometimes exacerbated by positive feedback loops when clear skies cause anomalous downward heat flux to warm the ocean's surface (Zaba & Rudnick, 2016; Zaba et al., 2020). Moreover, winds influence SST via vertical and horizontal heat advection, and SSTs influence wind speeds (Chelton et al., 2004; Small et al., 2008). Therefore, the coastal mode pattern may reflect a complex and covarying relationship between all three variables (SST, clouds/fog, and wind).

Although addressing the dynamical complexity of these interrelationships is beyond the scope of this study, we do emphasize our main finding that summer-averaged ocean temperatures and coastal land temperatures covary at similar amplitudes, suggesting a strong connection through the marine layer. The covarying relationship extends beyond Southern California. A cursory inspection of squared correlations between JAS-averaged Tmax and OISST at similar latitudes shows pockets of high correlations that correspond to coastal plains, bays, and in many cases urban areas, along the entire US West Coast (Figure 12). Further study is needed to quantify these relationships; however, since wind forcing is important for SST in this upwelling region, we hypothesize that wind-forced SST changes play a major role in the land-ocean heat exchange.

Returning to Southern California, we reemphasize the relationship between summer ocean temperatures and heat waves on land. To further illustrate this connection, we compare the SST time series in the SoCal Bight (Figure 6a), with the number of JAS heat wave days observed at SAN, LAX, LGB, and SBA stations averaged together. As the ocean surface temperature increases, so does the number of heat wave days (Figure 13), at a rate of 4.3 ± 1.0 heating days per °C of SST.

One of the strong correlations we find with A_2(t) is percent low cloud and fog cover. Schwartz et al. (2014) note that lagged correlations between SST and cloudiness on interannual timescales suggest that SSTs drive west coast low

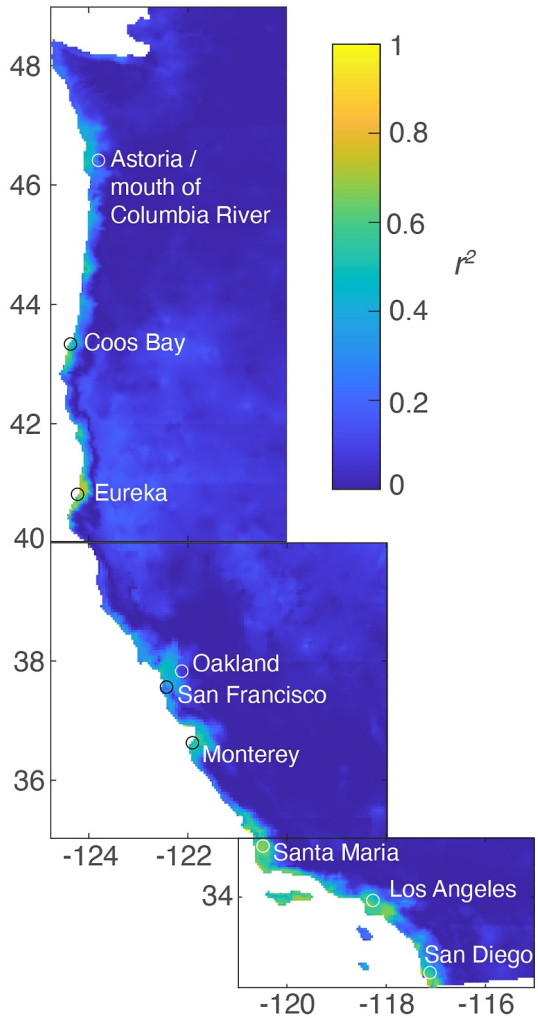

Figure 12. Correlation squared between JAS averages of OISST and Tmax along the U.S. West Coast for 1979–2021. The correlation is computed by choosing the OISST latitude grid line closest to a given Tmax grid point and computing the maximum OISST-Tmax correlation along that line over the 3 closest ocean points to the coast.

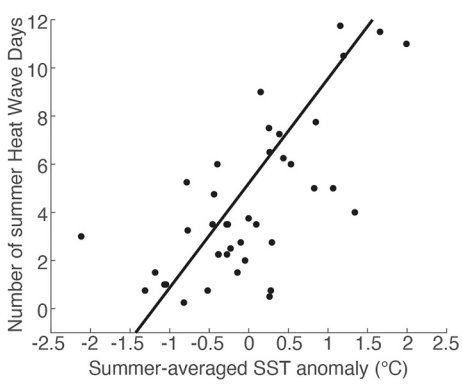

Figure 13. Scatter plot of average number of JAS heat wave days over four airport stations (SAN, LAX, LGB, SBA) versus JAS sea surface temperature anomaly ($r = 0.72$).

cloud and fog fluctuations. Over land along the California coastline, higher cloud albedo during the summer months (June–September) associates with both cooler daytime temperatures (Tmax) and warmer nighttime temperatures (Tmin), due to reflection of solar radiation and downwelling of infrared radiation, respectively (Iacobellis & Cayan, 2013). In Iacobellis and Cayan (2013), monthly mean cloud albedo during the summer at San Diego is found to correlate with changes in albedo over the ocean extending southward, similar to the high correlation pattern depicted in Figure 5b (Iacobellis & Cayan, 2013—see their Figure 8). Coastal low clouds and fog contribute to the high correlation between SST and the coastal mode because the degree of cloud/fog cover during the summer affects both ocean and land temperatures.

The presence or absence of coastal low clouds and marine layer fog undoubtedly drives coincident temperature changes on land and at the ocean surface (Iacobellis & Cayan, 2013); however, we hypothesize that the similar amplitudes of SST and A_2(t) land temperatures (Figure 6a) and the consistent increase in temperatures during day and night (Figure 8) indicate that the land-sea temperature changes likely are linked primarily through onshore exchange in the atmospheric marine layer, which is bounded by the coastal mountains. That is, changes in the marine layer temperature largely reflect changes in SST, and the onshore advection of marine layer air onto the SoCal coastal plain in summer in turn modulates the land temperatures, such that changes in Tmax resemble changes in SST. The role of clouds and fog contribute to these changes, but it seems unlikely that the resulting temperature changes would be so similar in amplitude over the land and ocean surfaces if they were not directly linked through the marine layer circulation. Moreover, if clouds and fog were the predominant reason for the ocean-atmosphere covariations in summer temperatures, the influence on temperature would be strongest during the day, as early morning marine layer conditions tend to dissipate in the heat of the day. Because temperatures at coastal zone stations show a similar change at all hours of the day (Figure 8b), this suggests that the surface ocean, with a high heat capacity, likely sets the primary cooling mechanism for land temperatures identified in this study.

Given the importance of coastal SSTs, the processes that determine the upper ocean heat balance during the summer warrant consideration. Wind-related mechanisms that may influence SST include changes in upwelling strength (Dorman & Palmer, 1981; Zaba et al., 2020), surface-heat flux (Fumo et al., 2020), wind-driven mixing at the base of the mixed layer (Fumo et al., 2020; Kantha & Clayson, 2002), and modulations of vertical advection due to changes in thermocline depth caused by remotely generated coastal-trapped waves (Wei et al., 2021). Since the wind anomalies associated with A_2(t) are relatively weak in the SoCal Bight and strong along the Baja California coast, wind-driven changes to mixed layer heat may occur primarily off Baja California, which then advect into the SoCal Bight, possibly via coastally trapped waves (Dong et al., 2009; Hickey et al., 2003; Pringle & Riser, 2003) or the Southern California Countercurrent (Dong et al., 2009), which is strongest from summer to fall (Hickey et al., 2003). In general, wind relaxations lead to the formation of poleward currents along the California coast (Melton et al., 2009; Send et al., 1987).

The importance of poleward advection to the upper ocean heat budget in the SoCal Bight seems plausible, but the evidence is uneven. Zaba et al. (2020) found that alongshore heat transport from the south, along with surface heat flux and vertical heat advection anomalies, contributed to the mixed layer heat

budget in the SoCal Bight during the anomalously warm conditions of 2014–2016. In contrast, Wei et al. (2021) found little contribution from alongshore heat transport during the 2018 MHW at Southern California. Poleward transport of warm water into the SoCal Bight also occurs during El Niño events (Frischknecht et al., 2015, 2017; Zaba et al., 2020), yet we find little correlation between mode 2 and ONI or Niño 3. Current and temperature observations south of San Diego would help to resolve the role of poleward flows in setting local SSTs. Further studies are necessary to fully understand the dynamical relationship behind the patterns uncovered between wind and SST, particularly in the region off the coast of Baja California.

We did not explore the nature of the inland mode 1 variability, other than to note a lack of correlation with the coastal variability linked to the coastal mode (winds, SST, clouds/fog), as our goal was specifically to understand the coastal region. However, we note that the North American Monsoon (NAM) impacts the study region, particularly the inland zone (east of the mountains), in the summer season (Moore et al., 2015). Though SoCal lies to the northwest of the core NAM region, cloud cover and precipitation from monsoon intrusions act to cool daytime high temperatures in the area (Adams & Comrie, 1997; NOAA, 2004), while free-tropospheric monsoonal moisture can reduce low cloud and fog cover in coastal SoCal (Clemesha et al., 2023). Further research is needed to establish NAM's influence on mode 1, and on other variability not captured by the two dominant EOF modes.

A relationship between conditions off Baja California and weather in SoCal has been noted in previous studies, though these studies focus on heat waves rather than seasonal mean Tmax. The changing "flavor" of heat waves in California (and Nevada) toward that of increased humidity has been linked to a particular region of the ocean just west of Baja California, which has seen a gradual enhanced warming of summertime SSTs and an increase in atmospheric moisture (Gershunov et al., 2009). Moisture from this source can advect into the southwestern US, where it enhances the nighttime temperature (Tmin) expression of heat events (Gershunov et al., 2009; Hulley et al., 2020).

We focused on the EOF of summer Tmax because it provided a clearer statistical separation of coastal and inland zones in the EOF analysis (as seen in Figure 3), which was not as strongly delineated in other variables and other times of year (e.g., JAS Tmin EOF, Spring Tmax EOF, 3-month moving average Tmax and Tmin EOFs). We note that an EOF of JAS Tmin (Figure S1 in Supporting Information S1) does produce a similar, albeit wider, coastal mode (mode 2); however, the JAS Tmin EOF is missing the corresponding "inverse," or inland, pattern in mode 1. Additionally, the variance explained by mode 2 is reduced in the JAS Tmin EOF to only 12.79% (compared to 24.99% for JAS Tmax). Choosing the late summer period deemphasized the importance of late spring to early summer clouds and fog, as well as the role of Santa Ana Wind events on coastal heat (Gershunov et al., 2021). Future work is needed to understand ocean-land temperature connections at intraseasonal time scales throughout the year. Additionally, our analysis does not consider variations of microclimates and levels of urbanization present within the coastal zone. The influence of the ocean on shorter time and smaller spatial scales requires further study. Future studies also are needed to evaluate the ability of regional coupled models to capture the summer land-ocean heat connection, to assess implications for climate projections in the region, and to understand the consequences of these findings for coastal residents of Southern California.

Data Availability Statement

Thirty arc s elevation data used in Figure 1 come from the GMTED2010 elevation data set (Danielson & Gesch, 2011) and are made available via USGS Earth Explorer: https://earthexplorer.usgs.gov/. The gridded air temperature data are available from gridMET (Abatzoglou, 2013) at https://www.climatologylab.org/gridmet.html. Station temperature data for San Diego International (SAN), Los Angeles International (LAX), Santa Barbara Municipal (SBA), and Long Beach (LGB) airports are available from the National Climatic Data Center (NCDC) Global Historical Climatology Network (GHCN) (Menne et al., 2012a, 2012b) using the Climate Data Online search tool, https://www.ncdc.noaa.gov/cdo-web/search. Hourly station temperature and wind data for San Diego International (SAN) (as well as for Los Angeles International Airport (LAX), Santa Barbara Municipal Airport (SBA), and Miramar Air Station (NKX)—all in Supplemental Materials only) are obtained through the Automated Surface Observing System (ASOS) (ASOS User's Guide, 1998) from Iowa Environmental Mesonet: https://mesonet.agron.iastate.edu/request/download.phtml?network=CA_ASOS. The Optimum Interpolation SST data are available from NOAA Physical Sciences Laboratory (Reynolds et al., 2002) at https://psl.noaa.gov/data/

gridded/data.noaa.oisst.v2.html. ERA5 wind data (Hersbach et al., 2020) are available at the Copernicus Climate Data Store: https://cds.climate.copernicus.eu/#!/home. The most recent cloud data analyzed in the current study were provided by coauthor Rachel Clemesha from NASA/NOAA Geostationary Operational Environmental Satellite (GOES) measurements, and are described in the 2016 paper "The northward march of summer low cloudiness along the California coast" (Clemesha et al., 2016), https://agupubs.onlinelibrary.wiley.com/doi/full/10.1002/2015GL067081. The cloud data are publicly available via the UCSD library repository https://doi.org/10.6075/J0RN3825 Temperature inversion data are available from NOAA Earth System Research Laboratories Radiosonde Database (Schwartz & Govett, 1992) at https://ruc.noaa.gov/raobs/. Oceanic Niño Index data are obtained from NOAA's Climate Prediction Center, https://origin.cpc.ncep.noaa.gov/products/analysis_monitoring/ensostuff/ONI_v5.php, based on Niño 3.4 region 3-month running-mean SST anomalies from a historical reconstructed SST analysis (Extended Reconstructed SST—ERSST.v5) (Huang et al., 2017). Niño 3 data are obtained from NOAA Physical Sciences Laboratory Global Climate Observing System (GCOS) Working Group on Surface Pressure (WG-SP), https://psl.noaa.gov/gcos_wgsp/Timeseries/Nino3/, calculated from the HadISST1 (Rayner et al., 2003). Pacific Decadal Oscillation index combines the Mantua PDO index (Mantua et al., 1997) with ERSST.v5 (Huang et al., 2017) and was obtained from the NOAA National Centers for Environmental Information, https://www.ncei.noaa.gov/access/monitoring/pdo/. North Pacific Gyre Oscillation data are obtained from Emanuele Di Lorenzo at Georgia Institute of Technology (Di Lorenzo et al., 2008) at http://www.o3d.org/npgo/.

Acknowledgments

This research was funded by the National Science Foundation's Coastlines and People (CoPe) program as part of the project "Heat waves in the Southern California coastal zone: Their oceanic and atmospheric drivers, human health impacts, and sustainable adaptation" (2209058). This study also was funded in part by the U.S. Army Corps of Engineers (W912HZ1920020) and the California Department of Parks and Recreation, Natural Resources Division Oceanography Program (C19E0026).

References

Abatzoglou, J. T. (2013). Development of gridded surface meteorological data for ecological applications and modelling. *International Journal of Climatology*, *33*(1), 121–131. https://doi.org/10.1002/joc.3413

Abatzoglou, J. T., Redmond, K. T., & Edwards, L. M. (2009). Classification of regional climate variability in the state of California. *Journal of Applied Meteorology and Climatology*, *48*(8), 1527–1541. https://doi.org/10.1175/2009JAMC2062.1

Adams, D. K., & Comrie, A. C. (1997). The North American monsoon. *Bulletin of the American Meteorological Society*, *78*(10), 2197–2214. https://doi.org/10.1175/1520-0477(1997)078<2197:TNAM>2.0.CO;2

Alfaro, E. J., Gershunov, A., & Cayan, D. (2006). Prediction of summer maximum and minimum temperature over the central and western United States: The roles of soil moisture and sea surface temperature. *Journal of Climate*, *19*(8), 1407–1421. https://doi.org/10.1175/JCLI3665.1

Archer, J. E., Luffman, I., Andrew Joyner, T., & Nandi, A. (2018). Identifying untapped potential: A geospatial analysis of Florida and California's 2009 recycled water production. *Journal of Water Reuse and Desalination*, *9*(2), 173–192. https://doi.org/10.2166/wrd.2018.012

Automated Surface Observing System (ASOS) User's Guide. (1998). National oceanic and atmospheric administration, Department of Defense, Federal Aviation Administration, U.S. Navy. Retrieved from https://www.weather.gov/media/asos/aum-toc.pdf

Chelton, D. B., Schlax, M. G., Freilich, M. H., & Milliff, R. F. (2004). Satellite measurements reveal persistent small-scale features in ocean winds. *Science*, *303*(5660), 978–983. https://doi.org/10.1126/science.1091901

Clemesha, R. E. S., Gershunov, A., Iacobellis, S. F., Williams, A. P., & Cayan, D. R. (2016). The northward march of summer low cloudiness along the California coast. *Geophysical Research Letters*, *43*(3), 1287–1295. https://doi.org/10.1002/2015GL067081

Clemesha, R. E. S., Guirguis, K., Gershunov, A., Small, I. J., & Tardy, A. (2018). California heat waves: Their spatial evolution, variation, and coastal modulation by low clouds. *Climate Dynamics*, *50*(11), 4285–4301. https://doi.org/10.1007/s00382-017-3875-7

Clemesha, R. E. S., Iacobellis, S. F., Gershunov, A., Cayan, D. R., Small, I. J., & Cavazos, T. (2023). North American monsoon impacts Southern California's coastal low clouds. *Geophysical Research Letters*, *50*(12), e2022GL102059. https://doi.org/10.1029/2022GL102059

Coles, S. (2001). *An introduction to statistical modeling of extreme values*. Springer Science & Business Media.

Danielson, J. J., & Gesch, D. B. (2011). *Global multi-resolution terrain elevation data 2010 (GMTED2010)*. USGS Numbered Series No. 2011–1073; Open-File Report (Vols. 2011–1073). U.S. Geological Survey. https://doi.org/10.3133/ofr20111073

Di Lorenzo, E., Schneider, N., Cobb, K. M., Franks, P. J. S., Chhak, K., Miller, A. J., et al. (2008). North Pacific Gyre Oscillation links ocean climate and ecosystem change. *Geophysical Research Letters*, *35*(8). https://doi.org/10.1029/2007GL032838

Dong, C., Idica, E. Y., & McWilliams, J. C. (2009). Circulation and multiple-scale variability in the Southern California Bight. *Progress in Oceanography*, *82*(3), 168–190. https://doi.org/10.1016/j.pocean.2009.07.005

Dorman, C. E., & Koračin, D. (2008). Response of the summer marine layer flow to an extreme California coastal bend. *Monthly Weather Review*, *136*(8), 2894–2922. https://doi.org/10.1175/2007MWR2336.1

Dorman, C. E., & Palmer, D. P. (1981). Southern California summer coastal upwelling. In *Coastal upwelling* (pp. 44–56). American Geophysical Union (AGU). https://doi.org/10.1029/CO001p0044

Dorman, C. E., & Winant, C. D. (2000). The structure and variability of the marine atmosphere around the Santa Barbara channel. *Monthly Weather Review*, *128*(2), 261–282. https://doi.org/10.1175/1520-0493(2000)128<0261:TSAVOT>2.0.CO;2

Durazo, R. (2015). Seasonality of the transitional region of the California Current System off Baja California. *Journal of Geophysical Research: Oceans*, *120*(2), 1173–1196. https://doi.org/10.1002/2014JC010405

Edinger, J. G. (1963). Modification of the marine layer over coastal Southern California. *Journal of Applied Meteorology and Climatology*, *2*(6), 706–712. https://doi.org/10.1175/1520-0450(1963)002<0706:MOTMLO>2.0.CO;2

Fewings, M. R., & Brown, K. S. (2019). Regional structure in the marine heat wave of summer 2015 off the western United States. *Frontiers in Marine Science*, *6*. https://doi.org/10.3389/fmars.2019.00564

Filonczuk, M. K., Cayan, D. R., & Riddle, L. G. (1995). Variability of marine fog along the California coast. Retrieved from https://escholarship.org/uc/item/2kc7x97f

Frischknecht, M., Münnich, M., & Gruber, N. (2015). Remote versus local influence of ENSO on the California Current System. *Journal of Geophysical Research: Oceans*, *120*(2), 1353–1374. https://doi.org/10.1002/2014JC010531

Frischknecht, M., Münnich, M., & Gruber, N. (2017). Local atmospheric forcing driving an unexpected California Current System response during the 2015–2016 El Niño. *Geophysical Research Letters*, *44*(1), 304–311. https://doi.org/10.1002/2016GL071316

Fumo, J. T., Carter, M. L., Flick, R. E., Rasmussen, L. L., Rudnick, D. L., & Iacobellis, S. F. (2020). Contextualizing marine heatwaves in the Southern California Bight under anthropogenic climate change. *Journal of Geophysical Research: Oceans*, *125*(5), e2019JC015674. https://doi.org/10.1029/2019JC015674

Gershunov, A., Cayan, D. R., & Iacobellis, S. F. (2009). The great 2006 heat wave over California and Nevada: Signal of an increasing trend. *Journal of Climate*, *22*(23), 6181–6203. https://doi.org/10.1175/2009JCLI2465.1

Gershunov, A., & Guirguis, K. (2012). California heat waves in the present and future. *Geophysical Research Letters*, *39*(18). https://doi.org/10.1029/2012GL052979

Gershunov, A., Guzman Morales, J., Hatchett, B., Guirguis, K., Aguilera, R., Shulgina, T., et al. (2021). Hot and cold flavors of southern California's Santa Ana winds: Their causes, trends, and links with wildfire. *Climate Dynamics*, *57*(7), 2233–2248. https://doi.org/10.1007/s00382-021-05802-z

Goss, M., Swain, D. L., Abatzoglou, J. T., Sarhadi, A., Kolden, C. A., Williams, A. P., & Diffenbaugh, N. S. (2020). Climate change is increasing the likelihood of extreme autumn wildfire conditions across California. *Environmental Research Letters*, *15*(9), 094016. https://doi.org/10.1088/1748-9326/ab83a7

Greene, C. (2024). Stipple. MATLAB Central File Exchange. https://www.mathworks.com/matlabcentral/fileexchange/68607-stipple

Guirguis, K., Basu, R., Al-Delaimy, W. K., Benmarhnia, T., Clemesha, R. E. S., Corcos, I., et al. (2018). Heat, disparities, and health outcomes in San Diego county's diverse climate zones. *GeoHealth*, *2*(7), 212–223. https://doi.org/10.1029/2017GH000127

Guirguis, K., Gershunov, A., Tardy, A., & Basu, R. (2014). The impact of recent heat waves on human health in California. *Journal of Applied Meteorology and Climatology*, *53*(1), 3–19. https://doi.org/10.1175/JAMC-D-13-0130.1

Hersbach, H., Bell, B., Berrisford, P., Hirahara, S., Horányi, A., Muñoz-Sabater, J., et al. (2020). The ERA5 global reanalysis. *Quarterly Journal of the Royal Meteorological Society*, *146*(730), 1999–2049. https://doi.org/10.1002/qj.3803

Hickey, B. M. (1979). The California current system—Hypotheses and facts. *Progress in Oceanography*, *8*(4), 191–279. https://doi.org/10.1016/0079-6611(79)90002-8

Hickey, B. M., Dobbins, E. L., & Allen, S. E. (2003). Local and remote forcing of currents and temperature in the central Southern California Bight. *Journal of Geophysical Research*, *108*(C3). https://doi.org/10.1029/2000JC000313

Huang, B., Thorne, P. W., Banzon, V. F., Boyer, T., Chepurin, G., Lawrimore, J. H., et al. (2017). Extended reconstructed sea surface temperature, version 5 (ERSSTv5): Upgrades, validations, and intercomparisons. *Journal of Climate*, *30*(20), 8179–8205. https://doi.org/10.1175/JCLI-D-16-0836.1

Hulley, G. C., Dousset, B., & Kahn, B. H. (2020). Rising trends in heatwave metrics across Southern California. *Earth's Future*, *8*(7), e2020EF001480. https://doi.org/10.1029/2020EF001480

Iacobellis, S., Cayan, D., Norris, J., & Kanamitsu, M. (2010). Impact of climate change on the frequency and intensity of low-level temperature inversions in California. Final Report to the California Air Resources Board Project 06-319. https://ww2.arb.ca.gov/sites/default/files/classic/research/apr/past/06-319.pdf

Iacobellis, S. F., & Cayan, D. R. (2013). The variability of California summertime marine stratus: Impacts on surface air temperatures. *Journal of Geophysical Research: Atmospheres*, *118*(16), 18–9122. https://doi.org/10.1002/jgrd.50652

Kalansky, J., Cayan, D., Barba, K., Walsh, L., Brouwer, K., & Boudreau, D. (2018). *California's fourth climate change assessment: San Diego region report*. (SUM-CCCA4-2018-009). University of California. Retrieved from https://www.energy.ca.gov/sites/default/files/2019-11/Reg_Report-SUM-CCCA4-2018-009_SanDiego_ADA.pdf

Kantha, L., & Clayson, C. (2002). Ocean mixed layer. In *Encyclopedia of atmospheric sciences* (p. 8). Retrieved from https://curry.eas.gatech.edu/Courses/6140/ency/Chapter11/Ency_Atmos/BL_Ocean_Mixed_Layer.pdf

Koračin, D., & Dorman, C. E. (2001). Marine atmospheric boundary layer divergence and clouds along California in June 1996. *Monthly Weather Review*, *129*(8), 2040–2056. https://doi.org/10.1175/1520-0493(2001)129<2040:MABLDA>2.0.CO;2

Lebassi-Habtezion, B., González, J., & Bornstein, R. (2011). Modeled large-scale warming impacts on summer California coastal-cooling trends. *Journal of Geophysical Research*, *116*(D20), D20114. https://doi.org/10.1029/2011JD015759

Lilly, D. K. (1968). Models of cloud-topped mixed layers under a strong inversion. *Quarterly Journal of the Royal Meteorological Society*, *94*(401), 292–309. https://doi.org/10.1002/qj.49709440106

Mantua, N. J., Hare, S. R., Zhang, Y., Wallace, J. M., & Francis, R. C. (1997). A Pacific interdecadal climate oscillation with impacts on Salmon production. *Bulletin of the American Meteorological Society*, *78*(6), 1069–1080. https://doi.org/10.1175/1520-0477(1997)078<1069:APICOW>2.0.CO;2

Masri, S., Jin, Y., & Wu, J. (2022). Compound risk of air pollution and heat days and the influence of wildfire by SES across California, 2018–2020: Implications for environmental justice in the context of climate change. *Climate*, *10*(10), 145. https://doi.org/10.3390/cli10100145

McEwen, G. F., & Brooks, C. F. (1923). How the Pacific Ocean affects Southern California's climate: Seasonal rainfall for 1923-24 indicated by ocean temperature. *Bulletin of the American Meteorological Society*, *4*(10), 142–148. https://doi.org/10.1175/1520-0477-4.10.142

Melton, C., Washburn, L., & Gotschalk, C. (2009). Wind relaxations and poleward flow events in a coastal upwelling system on the central California coast. *Journal of Geophysical Research*, *114*(C11). https://doi.org/10.1029/2009JC005397

Melton, F. S., Huntington, J., Grimm, R., Herring, J., Hall, M., Rollison, D., et al. (2022). OpenET: Filling a critical data gap in water management for the western United States. *Journal of the American Water Resources Association*, *58*(6), 971–994. https://doi.org/10.1111/1752-1688.12956

Menne, M. J., Durre, I., Korzeniewski, B., McNeill, S., Thomas, K., Yin, X., et al. (2012). Global historical climatology network—Daily (GHCN-Daily) (Version 3.30) [Dataset]. NOAA National Climatic Data Center. https://doi.org/10.7289/V5D21VHZ

Menne, M. J., Durre, I., Vose, R. S., Gleason, B. E., & Houston, T. G. (2012). An overview of the global historical climatology network-daily database. *Journal of Atmospheric and Oceanic Technology*, *29*(7), 897–910. https://doi.org/10.1175/JTECH-D-11-00103.1

Messner, S., Miranda, S. C., Young, E., & Hedge, N. (2011). Climate change-related impacts in the San Diego region by 2050. *Climate Change*, *109*(1), 505–531. https://doi.org/10.1007/s10584-011-0316-1

Moore, A. W., Small, I. J., Gutman, S. I., Bock, Y., Dumas, J. L., Fang, P., et al. (2015). National weather service forecasters use GPS precipitable water vapor for enhanced situational awareness during the Southern California summer monsoon. *Bulletin of the American Meteorological Society*, *96*(11), 1867–1877. https://doi.org/10.1175/BAMS-D-14-00095.1

Myers, T. A., Mechoso, C. R., Cesana, G. V., DeFlorio, M. J., & Waliser, D. E. (2018). Cloud feedback key to marine heatwave off Baja California. *Geophysical Research Letters*, *45*(9), 4345–4352. https://doi.org/10.1029/2018GL078242

NOAA. (2004). *The North American monsoon* (p. 25). National Oceanic and Atmospheric Administration. Retrieved from https://www.cpc.ncep.noaa.gov/products/outreach/Report-to-the-Nation-Monsoon_aug04.pdf

Oey, L.-Y. (1999). A forcing mechanism for the poleward flow off the southern California coast. *Journal of Geophysical Research*, *104*(C6), 13529–13539. https://doi.org/10.1029/1999JC900066

Perkins, S. E., Alexander, L. V., & Nairn, J. R. (2012). Increasing frequency, intensity and duration of observed global heatwaves and warm spells. *Geophysical Research Letters*, *39*(20). https://doi.org/10.1029/2012GL053361

Pierce, D. W., Kalansky, J. F., & Cayan, D. R. (2018). *Climate, drought, and sea level rise scenarios for California's fourth climate change assessment* (No. CCCA4-CEC-2018–006). California Energy Commission.

Planert, M., & Williams, J. S. (1995). *Ground water atlas of the United States: Segment 1, California, Nevada*. USGS Numbered Series No. 730-B; Hydrologic Atlas (Vols. 730-B, p. B1B28). U.S. Geological Survey. https://doi.org/10.3133/ha730B

Pringle, J. M., & Riser, K. (2003). Remotely forced nearshore upwelling in Southern California. *Journal of Geophysical Research*, *108*(C4). https://doi.org/10.1029/2002JC001447

Rasmussen, L. L., Carter, M. L., Flick, R. E., Hilbern, M., Fumo, J. T., Cornuelle, B. D., et al. (2020). A century of Southern California coastal ocean temperature measurements. *Journal of Geophysical Research: Oceans*, *125*(5), e2019JC015673. https://doi.org/10.1029/2019JC015673

Rayner, N. A., Parker, D. E., Horton, E. B., Folland, C. K., Alexander, L. V., Rowell, D. P., et al. (2003). Global analyses of sea surface temperature, sea ice, and night marine air temperature since the late nineteenth century. *Journal of Geophysical Research*, *108*(D14). https://doi.org/10.1029/2002JD002670

Reynolds, R. W., Rayner, N. A., Smith, T. M., Stokes, D. C., & Wang, W. (2002). An improved in situ and satellite SST analysis for climate. *Journal of Climate*, *15*(13), 1609–1625. https://doi.org/10.1175/1520-0442(2002)015<1609:AIISAS>2.0.CO;2

Robinson, C. J. (2016). Evolution of the 2014–2015 sea surface temperature warming in the central west coast of Baja California, Mexico, recorded by remote sensing. *Geophysical Research Letters*, *43*(13), 7066–7071. https://doi.org/10.1002/2016GL069356

Schwartz, B., & Govett, M. (1992). A hydrostatically consistent north American radiosonde data base at the Forecast Systems Laboratory, 1946-present (No. 4; NOAA Technical Memorandum ERL FSL). https://repository.library.noaa.gov/view/noaa/32850

Schwartz, R. E., Gershunov, A., Iacobellis, S. F., & Cayan, D. R. (2014). North American west coast summer low cloudiness: Broadscale variability associated with sea surface temperature. *Geophysical Research Letters*, *41*(9), 3307–3314. https://doi.org/10.1002/2014GL059825

Send, U., Beardsley, R. C., & Winant, C. D. (1987). Relaxation from upwelling in the Coastal Ocean Dynamics Experiment. *Journal of Geophysical Research*, *92*(C2), 1683–1698. https://doi.org/10.1029/JC092iC02p01683

Sequera, P., González, J. E., McDonald, K., Bornstein, R., & Comarazamy, D. (2015). Combined impacts of land cover changes and large-scale forcing on Southern California summer daily maximum temperatures. *Journal of Geophysical Research: Atmospheres*, *120*(18), 9208–9219. https://doi.org/10.1002/2015JD023536

Small, I. J. (2006). *Forecasters handbook for extreme southwestern California based on short term climatological approximations. Part I, The marine layer and its effect on precipitation and heating*. National Weather Service, Western Region., Scientific Services Division. Retrieved from https://repository.library.noaa.gov/view/noaa/14100

Small, R. J., deSzoeke, S. P., Xie, S. P., O'Neill, L., Seo, H., Song, Q., et al. (2008). Air–sea interaction over ocean fronts and eddies. *Dynamics of Atmospheres and Oceans*, *45*(3), 274–319. https://doi.org/10.1016/j.dynatmoce.2008.01.001

Vazquez, H. J., & Gomez-Valdes, J. (2018). Wind relaxation and poleward flow events in the upwelling region off Baja California, Mexico. *Ciencias Marinas*, *44*(2). https://doi.org/10.7773/cm.v44i2.2745

Wang, D., Deckter, E., Wong, T., & Wielicki, B. A. (2002). Sensitivities of cloud and radiation to changes in SST over the tropical eastern Pacific: Results from cloud-resolving simulations. *American Meteorological Society*. Retrieved from https://ams.confex.com/ams/pdfpapers/37894.pdf

Wei, X., Li, K.-Y., Kilpatrick, T., Wang, M., & Xie, S.-P. (2021). Large-scale conditions for the record-setting Southern California marine heatwave of August 2018. *Geophysical Research Letters*, *48*(7), e2020GL091803. https://doi.org/10.1029/2020GL091803

Winant, C. D., & Dorman, C. E. (1997). Seasonal patterns of surface wind stress and heat flux over the Southern California Bight. *Journal of Geophysical Research*, *102*(C3), 5641–5653. https://doi.org/10.1029/96JC02801

Zaba, K. D., & Rudnick, D. L. (2016). The 2014–2015 warming anomaly in the Southern California Current System observed by underwater gliders. *Geophysical Research Letters*, *43*(3), 1241–1248. https://doi.org/10.1002/2015GL067550

Zaba, K. D., Rudnick, D. L., Cornuelle, B. D., Gopalakrishnan, G., & Mazloff, M. R. (2018). Annual and interannual variability in the California current system: Comparison of an ocean state estimate with a network of underwater gliders. *Journal of Physical Oceanography*, *48*(12), 2965–2988. https://doi.org/10.1175/JPO-D-18-0037.1

Zaba, K. D., Rudnick, D. L., Cornuelle, B. D., Gopalakrishnan, G., & Mazloff, M. R. (2020). Volume and heat budgets in the coastal California Current System: Means, annual cycles, and interannual anomalies of 2014–16. *Journal of Physical Oceanography*, *50*(5), 1435–1453. https://doi.org/10.1175/JPO-D-19-0271.1